Author/s:
Phua, YL;Gilbert, T;Combes, A;Wilkinson, L;Little, MH

Title:
Neonatal vascularization and oxygen tension regulate appropriate perinatal renal medulla/papilla maturation

Date:
2016-04-01

Citation:
Phua, Y. L., Gilbert, T., Combes, A., Wilkinson, L. & Little, M. H. (2016). Neonatal vascularization and oxygen tension regulate appropriate perinatal renal medulla/papilla maturation. Journal of Pathology, 238 (5), pp.665-676. https://doi.org/10.1002/path.4690.

Persistent Link:
https://hdl.handle.net/11343/291071

15-725.R1 POULSOM EDITED ORIGINAL PAPER

Neonatal vascularisation and oxygen tension regulate appropriate perinatal renal medulla / papilla maturation

Yu Leng Phua[1,2,3], Thierry Gilbert[4], Alexander Combes[1,5,6], Lorine Wilkinson[1], Melissa H. Little[1,6,7,*]

[1]Institute for Molecular Bioscience, The University of Queensland, Brisbane, QLD, Australia

[2]Rangos Research Center, Children's Hospital of Pittsburgh of UPMC, Pittsburgh, PA, USA

[3]School of Medicine, Department of Pediatrics, Division of Nephrology, University of Pittsburgh, Pittsburgh, PA, USA

[4]Centre for Developmental Biology, University Paul Sabatier, Toulouse, France

[5]Department of Anatomy and Neuroscience, University of Melbourne, Melbourne, VIC, Australia

[6]Department of Pediatrics, University of Melbourne, Melbourne, VIC, Australia

[7]Murdoch Children's Research Institute, Royal Children's Hospital, Melbourne, VIC, Australia

Correspondence to:

Professor Melissa H. Little

NHMRC Senior Principal Research Fellow

Murdoch Children's Research Institute

Royal Children's Hospital

Melbourne, VIC, Australia

Email: melissa.little@mcri.edu.au

The authors have declared that no conflicts of interest exist.

This is the author manuscript accepted for publication and has undergone full peer review but has not been through the copyediting, typesetting, pagination and proofreading process, which may lead to differences between this version and the Version of Record. Please cite this article as doi: 10.1002/path.4690

Running title: Neonatal oxygenation regulates maturation of renal medulla/papilla {EdQ is this acceptable to authors?} I have made minor modification to the running title. It is OK now

Word count 3658

Expression microarray data are available on Gene Expression Omnibus, accession number: GSE72128 {EdQ release is a condition for publication} Microarray data has been released

Abstract

Congenital medullary dysplasia with obstructive nephropathy is a common congenital disorder observed in paediatric patients and represents the foremost cause of renal failure. However, the molecular processes regulating normal papillary outgrowth during the postnatal period are unclear. In this study, transcriptional profiling of the renal medulla across postnatal development revealed enrichment of non-canonical Wnt signalling, vascular development and planar cell polarity genes, all of which may contribute to perinatal medulla / papilla maturation. These pathways were investigated in a model of papillary hypoplasia with functional obstruction, the Crim1$^{KST264/KST264}$ transgenic mice. Postnatal elongation of the renal papilla via convergent-extension was unaffected in the Crim1$^{KST264/KST264}$ hypoplastic renal papilla. In contrast, these mice displayed a disorganised papillary vascular network, tissue hypoxia and elevated *Vegfa* expression. In addition, we demonstrate the involvement of accompanying systemic hypoxia arising from placental insufficiency, in appropriate papillary maturation. In conclusion, this study highlights the requirement for normal vascular development in collecting duct patterning, development of appropriate nephron architecture and perinatal papillary maturation, such that disturbances contribute to obstructive nephropathy. {EdQ please check that your meaning has been retained} OK

Keywords: Renal papilla, medullary vasculature, hypoxia, non-canonical Wnt signalling, convergent extension, Crim1

Introduction

Congenital Anomalies of the Kidney and Urinary Tract (CAKUT) are common genetic disorders that affect 1 in 200 humans, and represent the foremost cause of renal failure[1,2]. While CAKUT encompasses a diverse range of renal abnormalities, it is notable that congenital medullary dysplasia with obstructive nephropathy is one of the leading causes of renal failure in children [3,4]. Following obstructive filtrate accumulation within the renal parenchyma, pathological lesions including hydronephrosis and papillary atrophy ensue [5]. Atrophy of the renal papilla is widely believed to be a secondary pathological consequence following urinary obstruction, and emerging evidence has suggested that papillary anomalies may occur prior to the onset of urinary tract obstruction, thereby leading to inefficient urinary filtrate clearance[6].

Establishment of distinct cortical and medullary regions within the embryonic kidney is a tightly regulated process reported to involve multiple signalling pathways, including Wnt, integrin c-Met, renin-angiotensin and epidermal growth factor (Egf) signalling[7-11]. The role of Wnt signalling during embryonic renal cortico-medullary development is well established. Wnt7b secretion from the collecting duct signals to adjacent interstitium via a canonical ² -catenin pathway [7]. In response, the interstitium secretes Wnt4, Wnt5a and Wnt11 that act on the collecting ducts via a non-canonical Rho/Jnk pathway [7]. Such reciprocal interactions between the collecting duct and interstitium have been proposed to regulate collecting duct elongation via Planar Cell Polarity-Oriented Cell Division (PCP-OCD)[7]. Wnt9b can also act through the non-canonical Rho/Jnk pathway to direct PCP-OCD of the collecting ducts, as well as cellular convergent-extension during tubular extension[9]. Disruptions to the process of

PCP-OCD result in tubular cysts due to a perturbed plane of cellular division along the lumen axis[7,9]. These prior analyses have focused on prenatal organo-genetic events. We have previously demonstrated that the majority of papillary elongation and maturation occurs in the immediate postnatal period[6]. However, the signalling pathways and cellular processes involved in postnatal papillary elongation remain unclear.

In this study, expression profiling of postnatal medulla/papilla development identified non-canonical Wnt signalling, planar cell polarity/convergent extension, smooth muscle cell differentiation and vascular development as the major active pathways. Examination of a model of papillary hypoplasia, the Crim1$^{KST264/KST264}$ transgenic mice, highlighted defects in the formation of medullary vasculature in this phenotype, but did not reveal evidence implicating canonical Wnt signalling or convergent extension of the tubular epithelium. We have previously reported that a second *Crim1* transgenic line, the total Crim1$^{\Delta flox/\Delta flox}$ knockout model, differs from the Crim1$^{KST264/KST264}$ transgenic mice in that there is no accompanying placental insufficiency. In this study, we show that these mice did not develop papillary hypoplasia. However, a papillary hypoplasia phenotype can be induced in the Crim1$^{\Delta flox/\Delta flox}$ knockout model in response to intrauterine hypoxia. This emphasises the requirement for appropriate tissue oxygen tension for normal vascularisation and papillary maturation and implicates hypoxia as a modifier in medullary hypoplasia.

Materials and Methods

Mice

The Crim1$^{KST264/KST264}$, Crim1$^{\Delta flox/\Delta flox}$ knockout (Crim1CKO) and Bat-Gal transgenic mouse strains were maintained and genotyped as described previously [12-14]. All animal studies were performed in accordance to national guidelines with ethical approval from the University of Queensland Animal Ethics Committee (IMB/095/10/NHMRC NF). Time-mated wild type and Crim1CKO mice were subjected to 12% oxygen hypoxia from E11.5-18.5[15] and returned to normoxia at the time of littering. Kidneys were collected at 3 mo of age for analysis. Pyrvinium pamoate (Sigma) was reconstituted in DMSO and used at a concentration of 0.5mg/kg body weight. Daily intraperitoneal injections were performed in Bat-Gal mice from P2-6.

Sample preparation and microarray analysis

Regionally dissected renal medulla/papilla and cortex were obtained from a series of postnatal (P) male CD1 mice and submitted to the IMB SRC Microarray Facility for microarray profiling using Illumina MouseWG-6 v1 Expression BeadChips (Illumina). Total RNA was extracted using an RNeasy Mini Kit (Qiagen), followed by assessment of the quality and integrity of the RNA samples (Agilent RNA 6000 Nanochip (Agilent) Bioanalyzer). Intact RNA samples from four biological replicates were pooled in accordance to their respective experimental time points (P0, 2, 4, 6, 8, 10, 20, 30 and 90 d), thus a total of 36 medulla/papilla and cortex samples were analysed. Analysis of the microarray data was performed as previously described using lumi and limma packages (Bioconductor) in R, and genes with B-statistic>0 are considered statistically significant[16]. Bioinformatics analysis was performed using ToppFun[17] and GENE-E (Broad Institute). The microarray data are available on Gene Expression Omnibus, accession number: GSE72128.

Quantitative PCR analysis

cDNA was reverse-transcribed from equivalent amounts of total RNA with the use of a SuperScript® III First-Strand Synthesis System random priming method (Invitrogen) in accordance with the manufacturer's protocol[16,18], followed by standard SYBR Green quantitative PCR (qPCR) using a ViiA7 96-well Real Time PCR Platform (Applied Biosystems). Primers for qPCR are listed in Supplementary Table 1 and statistical analysis was performed by GraphPad Prism software with the use of Student's t-test.

Kidney histology, immunohistochemistry and immunofluorescence

Dissected kidneys were fixed in 4% w/v paraformaldehyde/PBS (PFA) overnight for paraffin sectioning, or 1h for X-gal staining and cryosectioning. Fixed kidney samples were stained in X-gal overnight at 37°C with constant agitation in standard X-gal staining solution [1X PBS, 2mM MgCl2, 5mM potassium ferrocyanide (K4Fe(CN)6-3H20) (Sigma), 5mM potassium ferricyanide (K3Fe(CN)6 (Sigma) pH7.2], supplemented with 0.01% sodium deoxycholate (Sigma), 0.02% NP-40 (Sigma) and 1mg/ml X-Gal (Invitrogen). X-gal stained samples were postfixed PFA overnight at 4°C then processed for paraffin sectioning. Bisection of kidneys for the papillary analysis was performed as previously described, and papillary length was normalised to overall kidney length[6]. To minimise technical bias in papillary base analysis, renal papillae were serially sectioned from tip to base, with the base sections used for immunohistochemistry. Standard immunohistochemistry, immunofluorescence, section *in situ* hybridization and Picrosirius red staining were performed as previously described[16,18,19]. Antibodies used at 1:100 dilution include Aqp2 (Millipore #AB3274), Aqp1 (Millipore #AB2219), Uromodulin (Biomedical Technologies Inc #BT-590), E-Cadherin (BD Pharmingen #610181), VE-Cadherin (BD Pharmingen #555289), ±SMA-FITC (Sigma #F3777) and NG2 (Millipore #AB5320). TUNEL (Roche) staining was performed in accordance to manufacturer's protocol. {EdQ please give clone/catalogue numbers and dilutions used for all primary Ab} Done

Wholemount immunofluorescence staining and Optical Projection Tomography

Wholemount immunofluorescence staining with the use of Calbindin antibody at 1:400 dilution (Sigma #C9848) and Optical Projection Tomography were performed as previously described on E14.5 wildtype and Crim1$^{KST264/KST264}$ kidneys[59].

Hypoxyprobe assessment of hypoxia

Hypoxyprobe™-1 (hpi, Hypoxyprobe Inc)/PBS was injected intraperitoneally at 200mg/kg into postnatal mice 2 h prior to euthanasia. To prevent post-mortem induced artefacts, all harvested kidneys were immediately snap frozen in liquid nitrogen, lysed in RIPA buffer and processed for western blotting. Antibodies used for the western blot include Hypoxyprobe-1 Mab1 FITC conjugated (Chemicon #90529, 1:1000), G3PDH (Trevigen #2275-PC-100, 1:3000) and anti-FITC secondary Mab clone 5D6.2 (Chemicon #90530, 1:5000). {EdQ please give clone/catalogue numbers and dilutions used for all primary Ab} Done

Scanning electron sample preparation and imaging

Bisected kidneys were fixed in 2.5% glutaraldehyde/PBS for 2hrs at room temperature, dehydrated in a PELCO Biowave microwave oven, critical point dried using a Tousimis Auto Critical Point Dryer, gold coated (SPI-MODULE Sputter Coater) and then imaged on a JEOL JCM5000 Benchtop SEM (Neoscope). All sample processing and scanning electron microscopy imaging was performed at the University of Queensland: Centre for Microscopy and Microanalysis (Australian Microscopy and Microanalysis Research Facilities).

Western blot analysis

P4 wildtype and Crim1$^{KST264/KST264}$ renal papillae were lysed in RIPA buffer and processed for western blotting. Antibodies used for the western blot include ²-catenin (Sigma #C2206, 1:1000) and G3PDH (Trevigen #2275-PC-100, 1:3000). {EdQ please give clone/catalogue numbers and dilutions used for all primary Ab} Done

Results

Analysis of differential pathway activity during postnatal renal papillary maturation

We have previously shown in the mouse that papillary elongation occurs in the immediate postnatal period, and that disruption to the process of papillary extension is associated with onset of functional obstruction and overt renal disease in the Crim1$^{KST264/KST264}$ mice[6]. The molecular regulation of renal papillary maturation during the immediate postnatal period is uncharacterised. We performed microarray expression profiling of the murine renal medulla (including papilla) versus renal cortex across postnatal development from day 0-90 in order to identify genes differentially expressed in the medulla. Hierarchical clustering of the medullary data revealed two distinct profile clusters consisting of early (P0-10) and late (P20-90) medulla/papilla development (Figure 1A). Given that papillary elongation occurs mostly in the immediate postnatal period we performed a comparison between early (P0-10) and late stage (P20-90) medullas, and identified 3,910 genes that were differentially expressed based on B-statistics (Supplementary Table 2). Next, we performed medulla versus cortex comparisons (P0-10) and identified genes that displayed clear temporal-spatial enrichment including, *Wnt4, Wnt7b, Wnt9b* in the medulla and *Wt1, Lhx1, Sox9* in cortex (Figure 1B and Supplementary Table 3-5). This agrees with published literature[7,19] including section *in situ* hybridization (SISH) from the GUDMAP database (www.gudmap.org)[20].

ToppFun bioinformatic analysis, performed on the top 200 differentially expressed genes (early vs. late medulla) showed enrichment for genes involved in vascular development (*Acta2, Thy1,*

Sema5a, Meis1, Shh, Pitx2), convergent extension (*Ptk7, Dcn, Nkd1, Robo1, Zeb2, Mmp14, Vangl2*), non-canonical Wnt signalling and Planar Cell Polarity (*Vangl2, Nkd1, Dact1, Ptk7, Gpc3*) (Figure 1C, D and Supplementary Table 6) in the early medulla. Similarly, ToppFun analysis of 121 genes (B-statistics >2) differentially enriched in the medulla versus cortex across P0 to P10 identified the strongest associations with vascular development and angiogenesis, reiterating the importance of these morphogenic events during immediately postnatal development of the medulla (Figure 1E and Supplementary Table 7).

Reduced collecting duct branching and nephron endowment in Crim1$^{KST264/KST264}$ occur without any evidence for convergent extension defects

Crim1$^{KST264/KST264}$ mice develop postnatal renal papillary hypoplasia leading to functional obstruction and interstitial fibrosis as consequence of this *Crim1* mutation[6]. Having identified transcripts differentially expressed within the normal postnatal medulla/papilla, we re-examined the Crim1$^{KST264/KST264}$ mice to determine which pathways contributed to this phenotype. QPCR analysis of differentially expressed medulla/papilla genes and previously described downstream targets[7,21-25] showed a significant reduction in expression of *Axin2, Lef1* (canonical Wnt target genes)*, Wnt11, Pod1, p57Kip2, Cnb1, Gas1,* ±*SMA* and *Pecam* within the Crim1$^{KST264/KST264}$ papilla which supports for the presence of an intrinsic papillary defect in these mice (Figure 2). Additionally, qPCR showed no changes in the expression of most Wnt ligands (*Wnt4, Wnt5a, Wnt9b, Wnt7b*).

To examine whether defects in development of prenatal nephrons or the ureteric tree contributed to the phenotype, analysis of papillary $Aqp1^{+}$ descending loops of Henle and $Aqp2^{+}$ collecting ducts was performed using immunohistochemistry. This revealed significantly fewer tubular structures across all P4-15 $Crim1^{KST264/KST264}$ postnatal mice, indicative of reduced nephron endowment (Figure 3A, B). We have shown recently that mild gestational hypoxia leads to a significant reduction (30-40%) of both nephron and ureteric tip number by E14.5[15]. Considering that the $Crim1^{KST264/KST264}$ mice display placental insufficiency[30], it was likely that tip number would be reduced. Optical Projection Tomography was used to assess ureteric tree branching in E14.5 $Crim1^{KST264/KST264}$ kidneys[27], revealing ~34% fewer ureteric tips as compared to wild type littermates (Supplementary Figure 1A and B). This supports a prenatal aetiology that includes gestational hypoxia. While it may be argued that a reduction in branching could contribute to papillary hypoplasia, many mouse models show a nephron deficit without evidence for papillary defects that lead to functional obstruction[15,31,32]. Additionally, immunostaining for $Aqp2^{+}$ collecting ducts and $Umod^{+}$ ascending loops of Henle on P4 $Crim1^{KST264/KST264}$ mid-sagittal kidney sections revealed defects in tubular descent from the cortico-medullary region into the papilla (Supplementary Figure 1C).

As non-canonical Wnt signalling/convergent extension was identified as potentially involved in postnatal medullary development, with evidence in the $Crim1^{KST264/KST264}$ mice of reduced expression of this pathway, we investigated whether there was evidence of perturbations to convergent extension in $Crim1^{KST264/KST264}$ mice. A comparison of wild type and

Crim1$^{KST264/KST264}$ neonates revealed clear evidence for collecting duct narrowing over time in both genotypes, suggesting that appropriate convergent extension was occurring within the papillary collecting ducts (Figure 3C). However, scanning electron microscopy revealed a striking mis-patterning of the Crim1$^{KST264/KST264}$ ducts of Bellini from the papillary tip, potentially representing an additional factor in the Crim1$^{KST264/KST264}$ obstructive phenotype (Figure 3D).

Canonical Wnt signalling is also likely to be dispensable for postnatal papillary elongation

Canonical Wnt signalling within the medullary interstitium has previously been shown to be indispensable for establishment of the cortico-medullary axis[7]. *Wnt7b* is enriched in the postnatal medulla, suggesting a requirement for active canonical Wnt signalling in this region, however there was no evidence for a reduction in *Wnt7b*, *Wnt4* or *Wnt5a* expression in the Crim1$^{KST264/KST264}$ mice. To investigate the role of canonical Wnt signalling in normal papillary elongation we analysed tissues from Bat-Gal lacZ reporter mice which express *lacZ* under the control of LEF/TCF responsive elements as a readout for canonical Wnt signalling[14]. Indeed, canonical Wnt signalling was spatially enriched within the renal medulla across all postnatal stages analysed (Supplementary Figure 2A). Sites of active canonical Wnt signalling were localised primarily within the medullary interstitium and a small fraction of Aqp2^{+} collecting ducts (Supplementary Figure 2B, C). However, canonical Wnt signalling activity was not present in Aqp1^{+} descending or Umod^{+} ascending loops of Henle, suggesting no involvement of this pathway in elongation of this compartment (Supplementary Figure 2D, E). Bat-Gal

mice were then given intraperitoneal injections of the GSK3β activator, pyrvinium pamoate[33,34], an inhibitor of canonical Wnt signalling, from P2 to P6 (Supplementary Figure 3). Knockdown of canonical Wnt activity was evident from the reduction in lacZ staining within the medullary region in all treated animals (Supplementary Figure 3A). This knockdown resulted in global renal hypoplasia, but with no effect on papillary length relative to kidney size (Supplementary Figure 3B, C), suggesting that this pathway is also dispensable for postnatal papillary development.

Crim1$^{KST264/KST264}$ postnatal renal papillae display vascular abnormalities and hypoxia

Microarray profiling revealed that vascular morphogenesis is highly active during early postnatal medullary development. Disruption to the vascularization process, as observed in *Sox17/Sox18* null mice, results in severe renal medullary dysplasia[35]. We have previously demonstrated that Crim1$^{KST264/KST264}$ mice develop multiple renal vascular abnormalities including leaky perivasculature, ectopic collagen accumulation within the endothelium and interstitial fibrosis[16,18,36]. Shh signalling from the collecting duct to the adjacent interstitium has previously been reported to be required for appropriate smooth muscle differentiation[37]. The microarray analyses identified components of Shh signalling in vascular development, but qPCR analyses showed no significant changes in *Shh, Ptch1, or Gli1,* or its downstream smooth muscle differentiation target genes including *Bmp4, Tshz3, Myocd* and *Pitx2* (Supplementary Figure 4)[37-39]. Nevertheless, it is possible that reduced

levels of ±*SMA, Pecam, Wnt11, Pod1, p57Kip2, Cnb1* and *Gas1* transcripts in the Crim1$^{KST264/KST264}$ papilla could also contribute towards the papillary vascular defects (Figure 2)[24,26-29].

In line with these vascular abnormalities, NG2 staining of the Crim1$^{KST264/KST264}$ papillary vasculature revealed severe disorganisation with expansion of the pericyte/interstitial vascular cells as early as P4, the earliest time point where papillary hypoplasia was observed in Crim1$^{KST264/KST264}$ mice (Figure 4A)[6]. Despite an expansion of NG2 pericyte/interstitial vascular cell population in the Crim1$^{KST264/KST264}$ papilla, reduced ±SMA density was observed, and is consistent with the reduced abundance of ±SMA transcripts (Supplementary Figure 5). This further supports an intrinsic abnormality in the capacity of the Crim1$^{KST264/KST264}$ papillary interstitium to adopt an appropriate smooth muscle cell fate during papillary vascular patterning. VE-Cadherin immunostaining of the endothelium also revealed a significant reduction in endothelial density, indicating the presence of an abnormal capillary network within the Crim1$^{KST264/KST264}$ renal papilla (Figure 4B and Supplementary Figure 6). The reduction in VE-Cadherin could perhaps be due to decreased ² -catenin[40] (Supplementary Figure 7), although Western blot analysis showed no significant changes in ² -catenin protein levels, further supporting a reduction in endothelial density rather than a perturbance of adherens junction formation.

Structural perturbations of the vasculature have previously been shown to result in tissue hypoxia due to inefficient oxygen transport[41]. To verify whether the disrupted vascular network within the Crim1$^{KST264/KST264}$ renal papilla results in tissue hypoxia, we performed SISH for *Vegfa*, a transcript that is commonly upregulated in response to hypoxia[42]. Stronger *Vegfa* signals were observed in Crim1$^{KST264/KST264}$ medullary collecting ducts at P4 (Figure 4C). In addition, intraperitoneal Hypoxyprobe injections into P4 Crim1$^{KST264/KST264}$ mice revealed significant accumulation of pimonidazole adducts[43] in the Crim1$^{KST264/KST264}$ kidneys (Figure 4D, 4E). Despite the hypoxic nature of the Crim1$^{KST264/KST264}$ kidneys, no overt apoptosis was observed in the renal papilla (Supplementary Figure 8). Together, these results indicate that perturbed vascularization and interstitial cell disruption resulting in tissue hypoxia are likely to be major contributing factors towards the Crim1$^{KST264/KST264}$ papillary hypoplasia.

In utero renal hypoxia and *Crim1* insufficiency result in Crim1$^{KST264/KST264}$ papillary hypoplasia and onset of chronic kidney disease

Crim1 is expressed in a temporal-spatial expression pattern within the papillary interstitium and loops of Henle during postnatal development[6,36,44]. Despite the known growth factor regulation of Crim1, the molecular mode of action of Crim1 within these papillary cell types is unknown. Indeed, the phenotypes of the Crim1$^{KST264/KST264}$ strain and a constitutionally deleted Crim1$^{\Delta flox/\Delta flox}$ knockout strain (Crim1 CKO) differ[13,36]. Both strains show glomerular abnormalities, although both papillary hypoplasia and placental defects are observed only in the Crim1$^{KST264/KST264}$ renal phenotype[6,30].

To determine whether placental insufficiency-induced intrauterine hypoxia resulted in the Crim1$^{KST264/KST264}$ papillary phenotype, we subjected time-mated Crim1CKO pregnant dams to hypoxia at 12% oxygen level throughout gestation. Adult wild type mice derived from pregnant dams exposed to normoxia or hypoxia (12% O_2) showed no signs of glomerular pathology or papillary hypoplasia (Figure 5). Similarly, adult Crim1CKO mutants from normoxic pregnant dams displayed no papillary hypoplasia (Figure 5). However, adult Crim1CKO mutants from hypoxia-treated pregnant dams developed pathological defects highly reminiscent of the Crim1$^{KST264/KST264}$ phenotype, including glomerular cysts, papillary hypoplasia and interstitial fibrosis (Figure 5). These results suggest that loss of *Crim1* within the kidney itself is insufficient for papillary dysplasia in Crim1$^{KST264/KST264}$ mice, with this phenotype influenced by oxygen tension during prenatal development.

Discussion

The processes and signalling pathways involved in elongation of the murine renal papilla during the postnatal period are unknown. Our previous studies showed that the postnatal defect in papillary maturation in Crim1$^{KST264/KST264}$ mice is associated with inefficient clearance of urinary filtrate, leading to functional obstruction and interstitial fibrosis[6]. In the present study, we identify vascular development as a major component of normal neonatal papillary development and provide evidence that the inappropriate patterning of the medullary vasculature and interstitium likely plays a significant role in the aetiology of papillary

hypoplasia in the Crim1$^{KST264/KST264}$ mice. Furthermore, we have shown that papillary hypoplasia in these mice results from a combination of the loss of Crim1 within the kidney and the accompanying gestational hypoxia resulting from the placental insufficiency.

Vasculogenesis and angiogenesis are important biological processes that are not only important for proper renal development, but are also implicated in renal diseases when dysregulated[45,46]. Our expression profiling data revealed a strong change of expression of genes in the second postnatal week. These genes include *Angpt2,* which is involved in Tie signalling and vascular remodelling[47], *Thy1* (CD90), a well-defined perivascular cells/Mesenchymal Stromal Cells marker[48,49], *Sema5a*, an axonal guidance cue which promotes angiogenesis[50], and *Pitx2* which is involved in vascular smooth muscle cell differentiation[39]. Other genes associated with postnatal medulla development, including *Shh*, *Tshz3* and *Klf5,* are also known to be involved in smooth muscle cell differentiation[37,38,51]. Indeed, multiple experimental models have reinforced the importance of vascular development with respect to renal papillary development. *Sox17/Sox18*-null mice develop medullary atrophy and hydronephrosis due to the absence of a proper medullary vascular network[35]. Similarly, use of the angiotensin II type I receptor antagonist, Candesartan, in postnatal rats led to downregulation of transcripts associated with angiogenesis including *Angpt1, Angpt2* and *Tie2* eventually leading to malformed medullary vasculature and thus smaller papillae[52]. Our microarray profiling of the postnatal developing renal medulla not only documents the active process of vascular morphogenesis at the transcript level, but also provides an insight into the temporal pattern of medullary vascular formation during the first 10 days of postnatal growth.

To investigate further the role of these pathways in papillary elongation, we examined the Crim1$^{KST264/KST264}$ mouse model, which displays vascular anomalies[18] and develops papillary hypoplasia leading to inefficient urinary filtrate clearance and hence functional obstruction[6]. Crim1 is a transmembrane protein that regulates the activity of multiple growth factors, including Bmp, Vegf and Pdgf family members[36,44]. Increased Bmp activity has previously been reported in the zebrafish to impede convergent-extension through downregulation of both Wnt11 and Wnt5a[53]. While it is conceivable that loss of Crim1 in our model would result in hyperactivation of the Bmp pathway, we show here that convergent-extension was unperturbed in the Crim1$^{KST264/KST264}$ hypoplastic renal papilla. This observation suggests that Crim1-mediated regulation of Bmp signalling is unlikely to be a critical player in the Crim1$^{KST264/KST264}$ renal papillary defects. Crim1 has also been shown to regulate VEGF signalling via the establishment of appropriate gradients of this growth factor during glomerular differentiation[36]. Given the severe disruption to the medullary vasculature, disruption to this growth factor are likely to be implicated. However, the phenotype of the Crim1$^{KST264/KST264}$ mice is complex, including severely disrupted medullary vasculature, mis-patterned ducts of Bellini and tissue hypoxia, suggesting perturbations to a number of Crim1-regulated pathways.

Crim1$^{KST264/KST264}$ mice, a mixed C57Bl6/CD1 gene trap line in which there is expression of an alternatively spliced form of the protein[12,36] also display placental insufficiency[30], whereas Crim1$^{\Delta flox/\Delta flox}$ knockout (Crim1CKO, mixed background), which mimics a total loss of Crim1 activity, is insufficient to recreate the placental or papillary phenotype[13]. This may

reflect background strain dependence or some form of dominant-negative activity in the Crim1$^{KST264/KST264}$ mice. Critically, the exposure of the Crim1CKO mice to mild gestational hypoxia recreated the papillary and interstitial fibrotic phenotype seen in Crim1$^{KST264/KST264}$ mice. More importantly, the findings revealed a critical requirement for both Crim1 genetic regulation and appropriate oxygen tension in final papillary development.

Previous studies have illustrated the contribution of both canonical and non-canonical Wnt signalling toward establishment of the embryonic renal medulla[7,9]. In this study, pyrvinium palmoate knockdown of canonical Wnt signalling did not result in significant perturbation of papillary elongation or cause formation of collecting duct cysts, suggesting that canonical Wnt signalling is dispensable for postnatal medullary development. In response to canonical Wnt7b activation from the collecting duct, the adjacent interstitial cells secrete Wnt4, Wnt5a and Wnt11 which are thought to regulate non-canonical PCP / oriented cell division of the collecting ducts prior to birth. However, collecting duct cells within the postnatal renal papilla are quiescent[54-57], suggesting that oriented cell division is not a critical driver of neonatal papillary elongation. The strong expression of non-canonical Wnt signalling genes implicated convergent extension within the collecting ducts as a potential driver of neonatal papillary elongation. Convergent extension remained evident in Crim1$^{KST264/KST264}$ mice despite a reduction in the expression of a number of Wnt target genes and the reduced expression of the *Wnt11* ligand. We hypothesise that non-canonical Wnt signalling is important for papillary elongation as this may also mediate collecting duct elongation via mediolateral intercalation of medullary interstitial cells into the postnatal collecting ducts, as previously reported[58].

In summary, we describe here the first comprehensive evaluation of differential medullary gene expression across the immediate postnatal period of kidney maturation in the mouse, highlighting vascularisation and canonical and non-canonical Wnt signalling. While these pathways were perturbed in a model of papillary hypoplasia, we show that defects in intrinsic vascular development accompanied by hypoxia contribute to papillary hypoplasia and interstitial fibrosis.

Acknowledgements

We acknowledge Bree Rumballe, Adler Ju (Little Lab, IMB/UQ), Kathryn Green (CMM), Charles Ferguson (Rob Parton Lab, IMB/UQ) for their technical assistance, Katia Nones (Sean Grimmond Lab, IMB/UQ) for the microarray data generation, Assoc. Prof. Karen Moritz (SBMS/UQ) for the hypoxia chamber and Dr. Jacqueline Ho (Children's Hospital of Pittsburgh of UPMC) for provision of technical resources. We acknowledge Shae Richardson and the support staff of The University of Queensland Biological Resources Animal Facility, SRC Microarray facility, ACRF/IMB Cancer Biology Imaging Facility and The University of Queensland Centre for Microscopy and Microanalysis-Australian Microscopy & Microanalysis Facility. YLP held an UQIRTA and UQRS scholarship. YLP is a George B. Rathmann Research Fellow supported by the ASN Ben J. Lipps Research Fellowship Program. MHL is an NHMRC Senior Principal Research Fellow (APP1042093).

Author Contributions:

YLP, TG, LW and MHL contributed intellectually to the design of the experiments. YLP, TG and AC performed the experiments and acquired data. YLP, LW and MHL analysed and interpreted the results. YLP, LW and MHL wrote the paper with editing and final approval from all authors.

Supplementary Information on the internet

Supplementary Figures 1-8

Figure S1. Reduced ureteric tree branching and perturbed nephron patterning in Crim1$^{KST264/KST264}$ kidneys.
Figure S2. Bat-Gal mice revealed the presence of canonical Wnt signalling within the medulla during postnatal development.
Figure S3. Canonical Wnt signalling is dispensable for postnatal medullary development.
Figure S4. Shh-associated genes implicated in smooth muscle differentiation were unaffected in the Crim1$^{KST264/KST264}$ papilla.
Figure S5. Reduced smooth muscle density in the Crim1$^{KST264/KST264}$ papilla.
Figure S6. Disrupted endothelium in the Crim1$^{KST264/KST264}$ papilla.
Figure S7. Crim1$^{KST264/KST264}$ papilla display normal levels of ² -catenin protein.
Figure S8. Crim1$^{KST264/KST264}$ papilla display appropriate tissue homeostasis.

Figure Legends

Figure 1. Microarray profiling of the postnatal developing kidney. (**A**) Hierarchal sample clustering of the microarray data revealed distinct clustering of P0-10 and P20-90 medullary samples. **(B)** Comparison of expression profiles between early medulla and matched cortex samples revealed 121 differentially expressed genes with B-statistics >2. **(C)** ToppFun biological processes curated from top 200 genes in early (P0-10) vs late (P20-90) medulla. **(D)** Genes involved in vascular development, convergent-extension and non-canonical Wnt signalling and Planar Cell Polarity are enriched in P0-10 medullary samples. **(E)** Top 13 ToppFun biological processes (13/736) from the early medulla vs. cortex gene expression comparison.

Figure 2. Quantitative PCR analysis of genes involved in medullary development. Significantly fewer *Axin2, Lef1, Wnt11, Pod1, p57Kip2, Cnb1, Gas1*, ±*SMA* and *Pecam* transcripts were observed in P4 $Crim1^{KST264/KST264}$ papilla. No differences were observed for *Wnt7b, Wnt9b, Wnt4* and *Wnt5a*. n=3, * p value<0.05, ** p value<0.01. Error bars represent standard error of the mean.

Figure 3. Renal papillary abnormalities in $Crim1^{KST264/KST264}$ mice. (A) Immunohistochemistry of P4-15 papillary bases revealed a reduction in $Aqp2^{+}$ collecting ducts and $Aqp1^{+}$ loops of Henle in the $Crim1^{KST264/KST264}$ papillary base. **(B)** Quantification revealed significantly fewer Aqp2+ and Aqp1+ tubules in the $Crim1^{KST264/KST264}$ papillary base. **(C)**

Convergent-extension of the Aqp2^{+} collecting ducts was observed in both wild type and Crim1$^{KST264/KST264}$ papilla base. **(D)** Scanning electron microscopy imaging of the papillary tip (double arrowheads and yellow dashed line) showed displacement of the Crim1$^{KST264/KST264}$ ducts of Bellini at all postnatal stages analysed. n=3, * p value<0.05, *** p value<0.001. Error bars represent standard deviation.

Figure 4. Defective medullary vascular development and hypoxia in Crim1$^{KST264/KST264}$ kidneys. (A) Immunofluorescence staining revealed abnormal expansion and distribution of NG2^{+} pericyte/interstitium within the P4 Crim1$^{KST264/KST264}$ papillary base (arrows). **(B)** Quantification revealed a significant reduction in VE-Cad^{+} density within the Crim1$^{KST264/KST264}$ papilla. n=3, *** p value<0.001. **(C)** Section *in situ* hybridization revealed upregulation of *Vegfa* within the P4 Crim1$^{KST264/KST264}$ papillary collecting ducts. Arrow denotes renal papilla. **(D and E)** Intraperitoneal injection of Hypoxyprobe followed by western blot and densitometric analysis showed significant accumulation of pimonidazole adducts in the P4 Crim1$^{KST264/KST264}$ kidneys n=3, * p value<0.05. Error bars represent standard error of the mean.

Figure 5. Intrauterine hypoxia and loss of *Crim1* results in increased disease severity and penetrance. (A) When subjected to hypoxia during gestation, Crim1CKO mice developed papillary hypoplasia and glomerular cysts (arrowheads) by 3 mo of age. No overt pathological abnormalities were observed in wild type mice when subjected to hypoxia. **(B)** Quantification

revealed a significant reduction in Crim1CKO papillary extension when subjected to hypoxia. Normoxia n=5, hypoxia n=4, * p value<0.05. No difference in papillary length was observed in wildtype mice when subjected to hypoxia. Normoxia n=5, hypoxia n=10, p value>0.05. Error bars represent standard error of the mean. **(C)** Picrosirius red staining of collagen fibres revealed evidence for fibrosis in hypoxia-treated Crim1CKO renal interstitium and extraglomerular regions.

References

1. Schedl A. Renal abnormalities and their developmental origin. *Nature Rev Genetics* 2007; **8**: 791-802.
2. Weber S, Moriniere V, Knüppel T*, et al.* Prevalence of mutations in renal developmental genes in children with renal hypodysplasia: Results of the ESCAPE Study. *J Am Soc Nephrol* 2006; **17**: 2864-2870.
3. Benfield MR, McDonald RA, Bartosh S*, et al.* Changing trends in pediatric transplantation: 2001 Annual Report of the North American Pediatric Renal Transplant Cooperative Study. *Pediatr Transpl* 2003; **7**: 321-335.
4. Klein J, Gonzalez J, Miravete M*, et al.* Congenital ureteropelvic junction obstruction: human disease and animal models. *Int J Exp Pathol* 2011; **92**: 168-192.
5. Chevalier RL, Forbes MS, Thornhill BA. Ureteral obstruction as a model of renal interstitial fibrosis and obstructive nephropathy. *Kidney Int* 2009; **75**: 1145-1152.
6. Wilkinson L, Kurniawan ND, Phua YL*, et al.* Association between congenital defects in papillary outgrowth and functional obstruction in Crim1 mutant mice. *J Pathol* 2012; **227**: 499-510.
7. Yu J, Carroll TJ, Rajagopal J*, et al.* A Wnt7b-dependent pathway regulates the orientation of epithelial cell division and establishes the cortico-medullary axis of the mammalian kidney. *Development* 2009; **136**: 161-171.
8. Zhang Z, Pascuet E, Hueber P-A*, et al.* Targeted Inactivation of EGF receptor inhibits renal collecting duct development and function. *J Am Soc Nephrol* 2010; **21**: 573-578.
9. Karner CM, Chirumamilla R, Aoki S*, et al.* Wnt9b signaling regulates planar cell polarity and kidney tubule morphogenesis. *Nature Genetics* 2009; **41**: 793-799.
10. Song R, Spera M, Garrett C*, et al.* Angiotensin II AT2 receptor regulates ureteric bud morphogenesis. *Am J Physiol Renal Physiol* 2010; **298**: F807-F817.
11. Liu Y, Chattopadhyay N, Qin S*, et al.* Coordinate integrin and c-Met signaling regulate Wnt gene expression during epithelial morphogenesis. *Development* 2009; **136**: 843-853.

12. Pennisi DJ, Wilkinson L, Kolle G*, et al. Crim1*$^{KST264/KST264}$ mice display a disruption of the Crim1 gene resulting in perinatal lethality with defects in multiple organ systems. *Developm Dynam* 2007; **236**: 502-511.
13. Chiu HS, York JP, Wilkinson L*, et al.* Production of a mouse line with a conditional Crim1 mutant allele. *Genesis* 2012; **50**: 711-716.
14. Maretto S, Cordenonsi M, Dupont S*, et al.* Mapping Wnt/² -catenin signaling during mouse development and in colorectal tumors. *Proc Natnl Acad Sci U S A* 2003; **100**: 3299-3304.
15. Wilkinson LJ, Neal CS, Singh RR*, et al.* Renal developmental defects resulting from in utero hypoxia are associated with suppression of ureteric beta-catenin signaling. *Kidney Int* 2015; **87**: 975-983.
16. Phua YL, Martel N, Pennisi DJ*, et al.* Distinct sites of renal fibrosis in Crim1 mutant mice arise from multiple cellular origins. *J Pathol* 2013; **229**: 685-696.
17. Chen J, Bardes EE, Aronow BJ*, et al.* ToppGene Suite for gene list enrichment analysis and candidate gene prioritization. *Nucl Acids Res* 2009; **37**: W305-W311.
18. Wilkinson L, Gilbert T, Sipos A*, et al.* Loss of renal microvascular integrity in postnatal Crim1 hypomorphic transgenic mice. *Kidney Int* 2009; **76**: 1161-1171.
19. Rumballe BA, Georgas KM, Combes AN*, et al.* Nephron formation adopts a novel spatial topology at cessation of nephrogenesis. *Developmental Biol* 2011; **360**: 110-122.
20. Harding SD, Armit C, Armstrong J*, et al.* The GUDMAP database – an online resource for genitourinary research. *Development* 2011; **138**: 2845-2853.
21. Quaggin SE, Schwartz L, Cui S*, et al.* The basic-helix-loop-helix protein Pod1 is critically important for kidney and lung organogenesis. *Development* 1999; **126**: 5771-5783.
22. Zhang P, Liegeois NJ, Wong C*, et al.* Altered cell differentiation and proliferation in mice lacking p57KIP2 indicates a role in Beckwith-Wiedemann syndrome. *Nature* 1997; **387**: 151-158.
23. Chang C-P, McDill BW, Neilson JR*, et al.* Calcineurin is required in urinary tract mesenchyme for the development of the pyeloureteral peristaltic machinery. *J Clin Invest* 2004; **113**: 1051-1058.

24. Spagnuolo R, Corada M, Orsenigo F*, et al.* Gas1 is induced by VE-cadherin and vascular endothelial growth factor and inhibits endothelial cell apoptosis. *Blood* 2004; **103**: 3005-3012.
25. Hellstrom M, Kal n M, Lindahl P*, et al.* Role of PDGF-B and PDGFR-beta in recruitment of vascular smooth muscle cells and pericytes during embryonic blood vessel formation in the mouse. *Development* 1999; **126**: 3047-3055.
26. Stefater Iii JA, Lewkowich I, Rao S*, et al.* Regulation of angiogenesis by a non-canonical Wnt-Flt1 pathway in myeloid cells. *Nature* 2011; **474**: 511-515.
27. Cui S, Schwartz L, Quaggin SE. Pod1 is required in stromal cells for glomerulogenesis. *Developm Dyn* 2003; **226**: 512-522.
28. Matsuura T, Takahashi K, Nakayama K*, et al.* Increased expression of vascular endothelial growth factor in placentas of p57Kip2 null embryos. *FEBS Letters* 2002; **532**: 283-288.
29. Graef IA, Chen F, Chen L*, et al.* Signals Transduced by Ca2+/Calcineurin and NFATc3/c4 Pattern the Developing Vasculature. *Cell* 2001; **105**: 863-875.
30. Pennisi DJ, Kinna G, Chiu HS*, et al.* Crim1 has an essential role in glycogen trophoblast cell and sinusoidal-trophoblast giant cell development in the placenta. *Placenta* 2012; **33**: 175-182.
31. Cullen-McEwen LA, Drago J, Bertram JF. Nephron endowment in glial cell line-derived neurotrophic factor (GDNF) heterozygous mice. *Kidney Int* 2001; **60**: 31-36.
32. O'Sullivan L, Cuffe JSM, Paravicini TM*, et al.* Prenatal exposure to dexamethasone in the mouse alters cardiac growth patterns and increases pulse pressure in aged male offspring. *PLoS ONE* 2013; **8**: e69149.
33. Venerando A, Girardi C, Ruzzene M*, et al.* Pyrvinium pamoate does not activate protein kinase CK1, but promotes Akt/PKB down-regulation and GSK3 activation. *Biochem J* 2013; **452**: 131-137.
34. Thorne CA, Hanson AJ, Schneider J*, et al.* Small-molecule inhibition of Wnt signaling through activation of casein kinase 1±. *Nature Chem Biol* 2010; **6**: 829-836.
35. Matsui T, Kanai-Azuma M, Hara K*, et al.* Redundant roles of Sox17 and Sox18 in postnatal angiogenesis in mice. *J Cell Sci* 2006; **119**: 3513-3526.

36. Wilkinson L, Gilbert T, Kinna G*, et al.* Crim1KST264/KST264 mice implicate Crim1 in the regulation of vascular endothelial growth factor-A activity during glomerular vascular development. *J Am Soc Nephrol* 2007; **18**: 1697-1708.
37. Yu J, Carroll TJ, McMahon AP. Sonic hedgehog regulates proliferation and differentiation of mesenchymal cells in the mouse metanephric kidney. *Development* 2002; **129**: 5301-5312.
38. Caubit X, Lye CM, Martin E*, et al.* Teashirt 3 is necessary for ureteral smooth muscle differentiation downstream of SHH and BMP4. *Development* 2008; **135**: 3301-3310.
39. Shang Y, Yoshida T, Amendt BA*, et al.* Pitx2 is functionally important in the early stages of vascular smooth muscle cell differentiation. *J Cell Biol* 2008; **181**: 461-473.
40. Lampugnani MG, Corada M, Caveda L*, et al.* The molecular organization of endothelial cell to cell junctions: differential association of plakoglobin, beta-catenin, and alpha-catenin with vascular endothelial cadherin (VE-cadherin). *J Cell Biol* 1995; **129**: 203-217.
41. Rong Y, Durden DL, Van Meir EG*, et al.* 'Pseudopalisading' necrosis in glioblastoma: a familiar morphologic feature that links vascular pathology, hypoxia, and angiogenesis. *J Neuropathol Exp Neurol* 2006; **65**: 529-539.
42. Shweiki D, Itin A, Soffer D*, et al.* Vascular endothelial growth factor induced by hypoxia may mediate hypoxia-initiated angiogenesis. *Nature* 1992; **359**: 843-845.
43. Raleigh JA, Miller GG, Franko AJ*, et al.* Fluorescence immunohistochemical detection of hypoxic cells in spheroids and tumours. *Br J Cancer* 1987; **56**: 395-400.
44. Wilkinson L, Kolle G, Wen D*, et al.* CRIM1 regulates the rate of processing and delivery of bone morphogenetic proteins to the cell surface. *J Biol Chem* 2003; **278**: 34181-34188.
45. Lindahl P, Hellstrom M, Kalen M*, et al.* Paracrine PDGF-B/PDGF-Rbeta signaling controls mesangial cell development in kidney glomeruli. *Development* 1998; **125**: 3313-3322.
46. Eremina V, Cui S, Gerber H*, et al.* vascular endothelial growth factor a signaling in the podocyte-endothelial compartment is required for mesangial cell migration and survival. *J Am Soc Nephrol* 2006; **17**: 724-735.

47. Cines DB, Pollak ES, Buck CA*, et al.* Endothelial cells in physiology and in the pathophysiology of vascular disorders. *Blood* 1998; **91**: 3527-3561.
48. Crisan M, Yap S, Casteilla L*, et al.* A perivascular origin for mesenchymal stem cells in multiple human organs. *Cell Stem Cell* 2008; **3**: 301-313.
49. Dominici M, Le Blanc K, Mueller I*, et al.* Minimal criteria for defining multipotent mesenchymal stromal cells. The International Society for Cellular Therapy position statement. *Cytotherapy* 2006; **8**: 315-317.
50. Sadanandam A, Rosenbaugh EG, Singh S*, et al.* Semaphorin 5A promotes angiogenesis by increasing endothelial cell proliferation, migration, and decreasing apoptosis. *Microvasc Res* 2010; **79**: 1-9.
51. Nagai R, Shindo T, Manabe I*, et al.* KLF5/BTEB2, a Kruppel-like zinc-finger type transcription factor, mediates both smooth muscle cell activation and cardiac hypertrophy. *Adv Exp Med Biol* 2003; **538**: 57-66.
52. Madsen K, Marcussen N, Pedersen M*, et al.* Angiotensin II promotes development of the renal microcirculation through AT1 Receptors. *J Am Soc Nephrol* 2010; **21**: 448-459.
53. Myers DC, Sepich DS, Solnica-Krezel L. Bmp activity gradient regulates convergent extension during zebrafish gastrulation. *Developm Biol* 2002; **243**: 81-98.
54. Oliver JA, Maarouf O, Cheema FH*, et al.* The renal papilla is a niche for adult kidney stem cells. *J Clin Invest* 2004; **114**: 795-804.
55. Adams DC, Oxburgh L. The long-term label retaining population of the renal papilla arises through divergent regional growth of the kidney. *Am J Physiol- Renal Physiol* 2009; **297**: F809-F815.
56. Oliver JA, Klinakis A, Cheema FH*, et al.* Proliferation and migration of label-retaining cells of the kidney papilla. *J Am Soc Nephrol* 2009; **20**: 2315-2327.
57. Song J, Czerniak S, Wang T*, et al.* Characterization and fate of telomerase-expressing epithelia during kidney repair. *J Am Soc Nephrol* 2011; **22**: 2256-2265.
58. Li J, Ariunbold U, Suhaimi N*, et al.* Collecting duct-derived cells display mesenchymal stem cell properties and retain selective in vitro and in vivo epithelial capacity. *J Am Soc Nephrol* 2015; **26**: 81-94.

59. Short Kieran M, Combes Alexander N, Lefevre J*, et al.* Global quantification of tissue dynamics in the developing mouse kidney. *Developm Cell* 2014; **29**: 188-202.

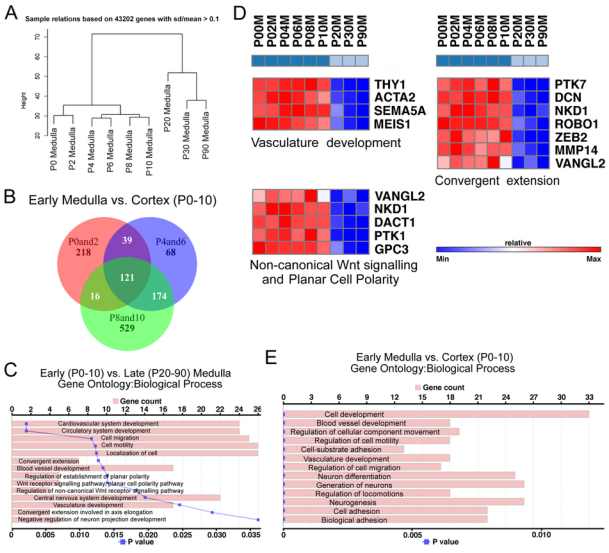

Fig1_Microarray_early_vs_late RP.tif

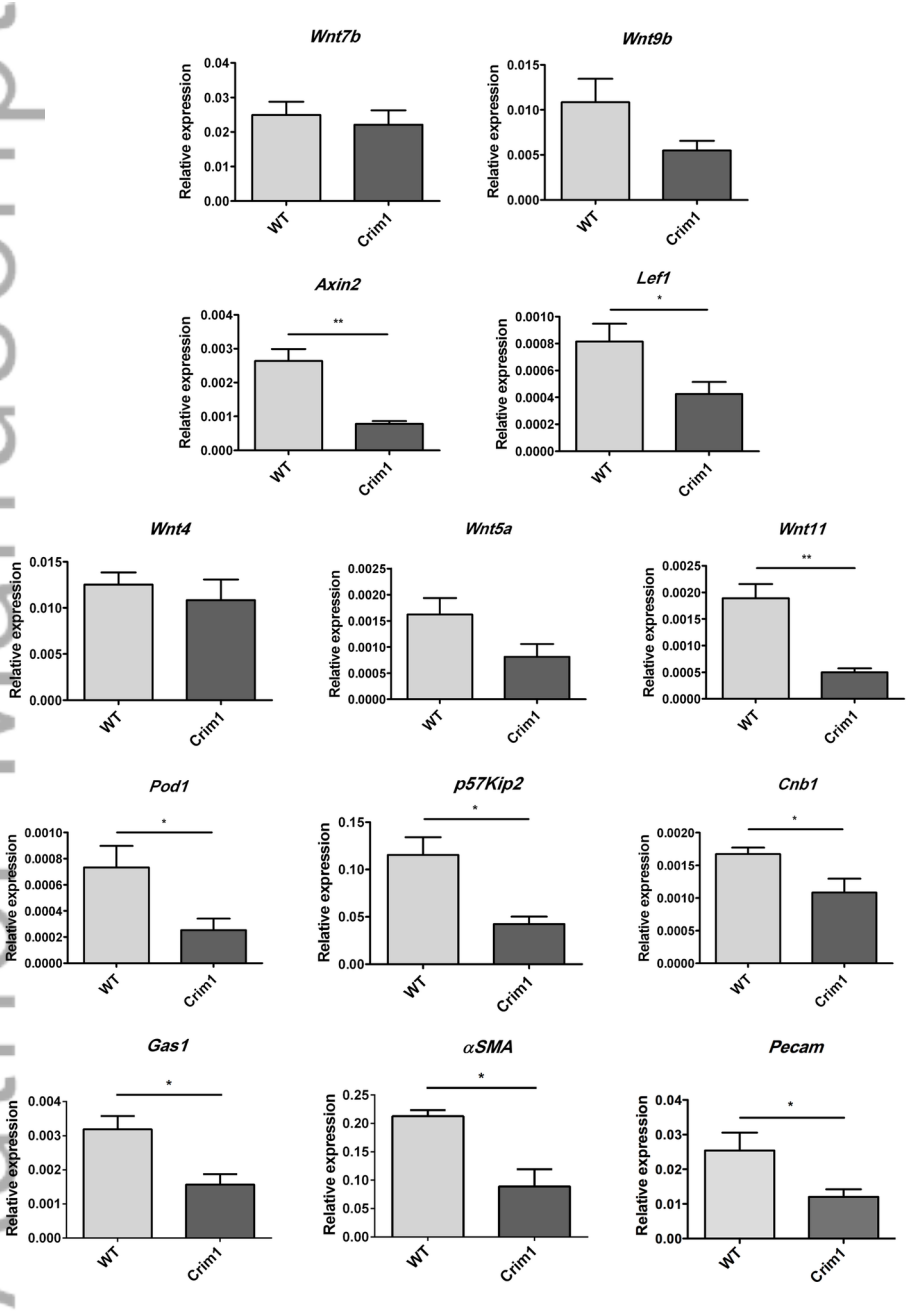

Fig2_qPCR_revised2 RP.tif

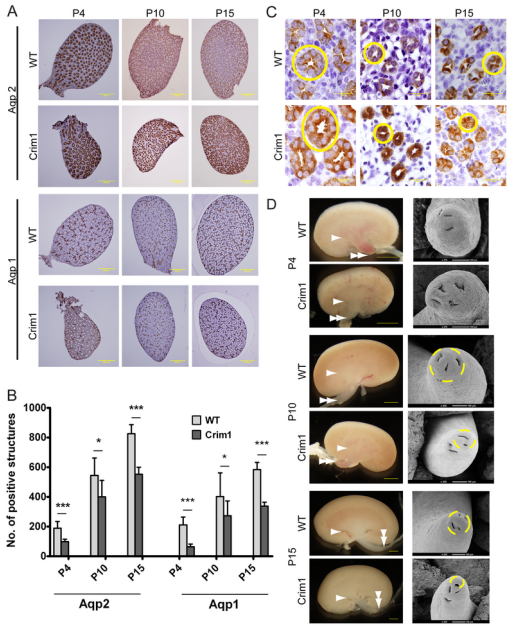

Fig3 Papilla abnormalities.tif

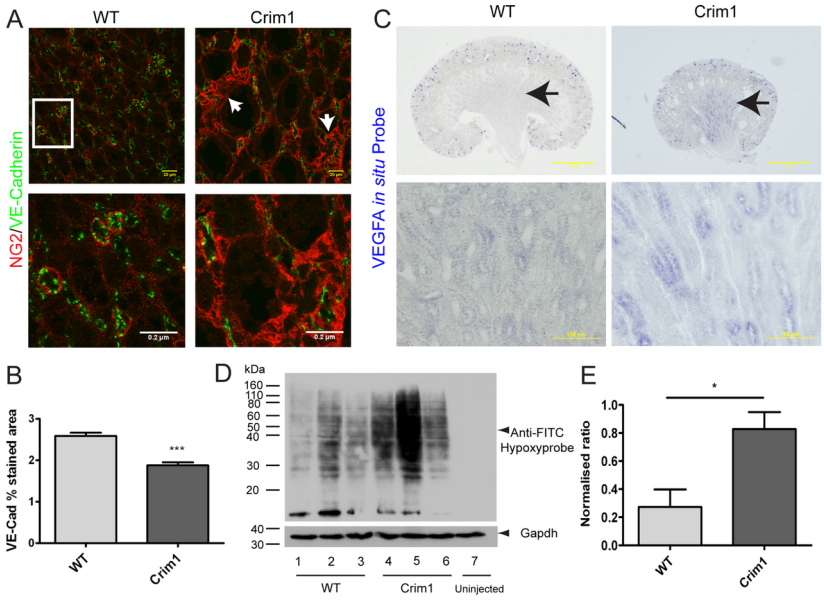

Fig4 Papilla vascular abnormalities edited.tif

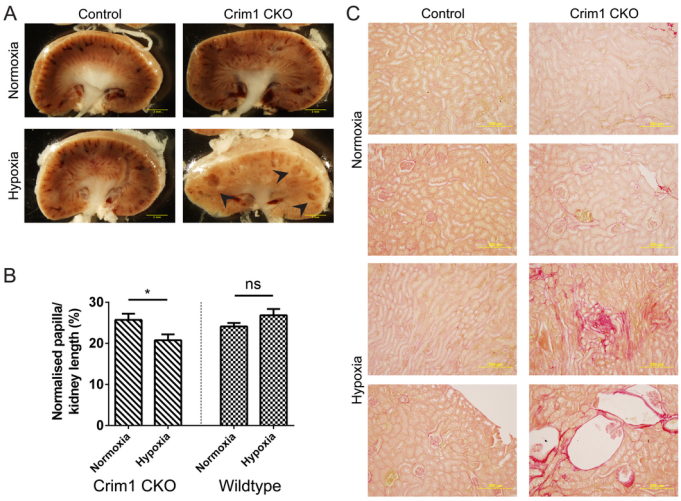

Fig5_CKO_Normoxia_Hypoxia RP.tif